Korean J. Chem. Eng., 39(3), 562-575 (2022)
DOI: 10.1007/s11814-021-0961-7

pISSN: 0256-1115
eISSN: 1975-7220

Experimental investigation of nanofluid injection assisted microwave radiation for enhanced heavy oil recovery in a micromodel system

Reza Gharibshahi*, Mohammadreza Omidkhah*,†, Arezou Jafari*,†, and Zahra Fakhroueian**

*Faculty of Chemical Engineering, Tarbiat Modares University, Tehran, Iran
**School of Chemical Engineering, College of Engineering, Institute of Petroleum Engineering, University of Tehran, Tehran, Iran

(*Received 8 July 2021 • Revised 29 August 2021 • Accepted 16 September 2021*)

Abstract−Microwave (MW) absorption ability of Fe_3O_4 nanoparticles was increased by attaching NiO nanomaterials to them through a co-precipitation approach. The surface of the synthesized nanohybrids was hydrophilized using three different natural agents to disperse in water. The synthesized nanohybrids were characterized by several analyses. The colloidal stability, magnetic behavior and the effect of surface modification agent on the MW absorption ability of the synthesized nanohybrids were investigated. The ability of surface-modified nanohybrids to increase the oil recovery factor was studied by injecting them into a 2D glass micromodel as the porous medium. The results showed that CA is the best modification agent with high colloidal stability, strong MW absorption and the lowest effect on the reduction of magnetic saturation of uncoated nanohybrids. Citric acid decreased the saturation magnetization from 55.43 emu/gr at the uncoated state to 52.82 emu/gr at the modified state. The oil sample with more polar compounds such as asphaltene could be further heated and its viscosity further reduced in an EM heating process. By adding 0.1 wt% of the Fe_3O_4-NiO nanohybrids, the viscosity of sample (S1) was reduced by 266 mPa·s more than the MW radiation state alone. The findings indicate that MW radiation can significantly increase the heavy oil recovery factor. Water injection had only 16.6% oil recovery; however, this value increased to 41.5% by radiating 400 watts MW. This increase will be further enhanced by adding modified Fe_3O_4-NiO nanohybrids to water. The Fe_3O_4-NiO @ CA, Fe_3O_4-NiO @ APTES, and Fe_3O_4-NiO @ PEG had 69%, 63.5%, and 58.3% oil recovery, respectively. Finally, it was found that the surface modified nanohybrids could change the wettability of the porous medium from oil-wet to water-wet. After coating the glass with the Fe_3O_4-NiO @ CA nanofluid, the oil contact angle decreased from 140° to 17°.

Keywords: Fe_3O_4-NiO Nanohybrids, Surface Modification, Microwave Radiation, Micromodel, Oil Recovery Factor

INTRODUCTION

Heavy and extra-heavy oil extraction is a challenging issue in the oil industry [1]. Due to high oil viscosity, oil extraction from these reservoirs is difficult, and transport and refining is costly. High levels of sulfur, heavy metals, carbon dioxide, and nitrogen content in these types of oils have raised environmental concerns caused by their refining [2]. On the other hand, oil recovery from these reservoirs is poor and its world market prices are much lower than light crude oil [1,3]. Therefore, it is important to improve the quality of heavy oils and increase their production capacity due to the rising demand for energy in the future.

Generally, recovery of residual and unproductive oil from heavy oil reservoirs is achieved using thermal enhanced oil recovery (EOR) methods. These methods entail conventional approaches such as steam and hot water injection, combustion, steam-assisted gravity drainage (SAGD), and newer methods like EM heating [4-8]. The basis of all these methods is to heat a greater volume of a reservoir optimally. Raising the oil temperature reduces the viscosity of oil and improves its ability to move in the reservoir and towards the production well [9,10]. Conventional methods are not compatible with all types of reservoirs and do not typically satisfy economic and environmental issues [11,12]. In recent years, EM heating or radiofrequency heating (RF) has shown promising signs for overcoming the disadvantages of conventional methods in conducted research. [4,5,13-15]. Compared to the conventional thermal EOR methods, the EM heating process is a precise, controllable, economically feasible, environmentally friendly, and selective heating process with the least lost energy into the reservoir. Besides, the EM heating process has high compatibility with diverse types of reservoirs and a short process time to heat the production zone.

EM heating is classified into three categories, according to the frequency ranges (from 3 kHz to 300 GHz): ohmic or resistive heating with low frequency, induction heating with medium frequency, and high frequency or MW radiation [5]. In MW radiation, the dominant heating mechanism is dielectric heating [16]. Microwaves increase the internal energy of a substance by stimulating dielectric reactions and creating atomic polarization within it [17]. As a result, the temperature of the material increases. Thus, unlike conventional thermal conduction and convection heating methods, microwaves can heat materials without physical contact in less time [5,7]. Experimental studies showed that the total energy efficiency of MW heating could be approximately 80%. Chemical reactions using MW occur up to 10-1,000 times faster than conventional

†To whom correspondence should be addressed.
E-mail: omidkhah@modares.ac.ir, ajafari@modares.ac.ir
Copyright by The Korean Institute of Chemical Engineers.

methods. MW heating consumes the lowest energy compared with different electrical heating methods [5,18,19].

Using the MW radiation method, it should be borne in mind that any substance is not able to absorb microwaves [20]. For example, crude oil is not a suitable absorbent of microwaves [19,21]. However, by increasing the number of polar components, such as asphaltene and resin molecules, the ability of crude oil to absorb microwaves increases. Microwaves have a low penetration depth. Therefore, the stimulated area inside the reservoir can be reduced [22]. To overcome these difficulties, using additional materials like nanoparticles is an appropriate way to enhance the performance and decrease the expense of using this technique in field operations [23]. Using high MW absorbent nanomaterials dispersed in the injected fluid would absorb a greater amount of radiated energy [23,24]. Consequently, transferring heat energy from injected fluid to crude oil can warm up a more significant reservoir volume [25,26].

Nanoparticles possess special properties, including small size, high surface area, high dispersibility, and catalytic activity, and high strength [27,28]. Different laboratory studies are required to determine the best nanoparticle and to find comprehensive and accurate information about the process of MW radiation coupled with nanofluid injection [29,30]. Several nanostructured materials, including metallic nanoparticles, carbon nanomaterials, and zeolites, were used in previous studies [31-36]. Using MW radiation process coupled with nanofluid injection has different effects on an oil reservoir; for example, decreasing the viscosity of crude oil or bitumen, changing the wettability of rock reservoir, separating the oil and water into the reservoir, and increasing the oil recovery factor in an EOR operation [19,23,26,31,33-35,37-41]. Given the efforts made, the best type of nanoparticle and its injection conditions and the mechanism of their effect on the process are still unclear.

Magnetic nanoparticles showed desired potentials for use in all areas of the petroleum industry like oilfield applications [42]. Regarding the literature, superparamagnetic iron oxide (Fe_3O_4) nanoparticles have a better potential for use in this process than other nanoparticles [43]. Nevertheless, they can trigger the magnetic loss term of EM-waves and have a poor ability to absorb the dielectric loss of EM-waves [20]. Mixing a material with another strong MW absorbent by coating, doping, cladding, and modifying can increase their ability to absorb MW energy [17].

Therefore, in this study, Fe_3O_4 (Iron oxide) nanoparticles were hybridized with NiO (nickel oxide) nanomaterials to improve the MW absorbing capacity and their performance in an MW radiation operation. Fe-Ni hybrid possesses suitable EM absorption properties in a specific frequency band due to its excellent magnetically soft properties such as morphology variability, complex permeability, and permittivity [20]. Hence, this alloy is widely employed in electronic devices. Fe_3O_4-NiO nanohybrids were treated with three specific modification agents including citric acid (CA), (3-aminopropyl)triethoxysilane (APTES), and polyethylene glycol (PEG 6000) to yield hydrophilic particles. The characteristics of modified/unmodified nanohybrids were investigated using various analyses: Fourier transform infrared spectroscopy (FTIR), X-Ray Diffraction (XRD), field emission scanning electron microscopy (FESEM), energy dispersive X-ray spectrometry (EDX), and vibrating sample magnetometer (VSM). The stability of the synthesized nanohybrids in water, the injected fluid in the EOR process, and their ability to absorb EM waves were quantitatively and qualitatively determined. In the next stage, the effect of oil type (three oil samples with different asphaltene content) on the amount of MW absorption of synthesized nanohybrids was investigated. This analysis was done to find the capability of the synthesized nanohybrids for use in different oil reservoirs. Finally, several micromodel injection tests were performed to explore the ability of the modified nanohybrids in the EM heating process in order to boost the oil recovery factor. Herein, we attempted to find the best surface modification agent with high stability and strong performance in the EM heating process.

MATERIALS AND METHODS

1. Materials

$FeCl_3{\cdot}6H_2O$, $FeCl_2{\cdot}4H_2O$, ammonia solution (NH_4OH), sodium hydroxide solution (NaOH), toluene (C_7H_8), and trichloromethylsilane (CH_3Cl_3Si) purchased from the Merck Company were used for synthesizing Fe_3O_4 nanoparticles and applying oil-wetting condition in the micromodel. NiO nanoparticles with 20 nm diameter were supplied from US Research Nanomaterials to hybridize with Fe_3O_4 nanoparticles. CA ($C_6H_8O_7$), (3-aminopropyl)triethoxysilane (APTES, $C_9H_{23}NO_3Si$), polyethylene glycol 6000 (PEG, $H(OCH_2CH_2)_nOH$) as the modification agents were provided from Titrachem Company. Nitrogen (N_2) flow with high purity was used as an anti-oxidant throughout the synthesis process. Deionized (DI) distilled water was used during the tests as the dispersion medium, solvent, and washing fluid.

Three oil samples from different Iranian oil reservoirs were prepared for use in the static and dynamic EM-absorption and micromodel flooding tests. The properties of oil samples are in Table 1.

2. Synthesis of Fe_3O_4-NiO Nanohybrid

Fe_3O_4-NiO nanohybrid with a weight ratio of 3 : 1 was synthesized *via* a co-precipitation method with some modifications [44,45]. For this purpose, 1 g of NiO nanoparticles was sonicated in 200 ml of DI-water at maximum power for 30 min. Then, $FeCl_3{\cdot}6H_2O$ (7 g, 25.9 mmol) and $FeCl_2{\cdot}4H_2O$ (2.57 g, 12.95 mmol) were added to the solution in a three-bottleneck flask. The obtained solu-

Table 1. The properties of oil samples at ambient pressure and temperature (1 atm. 25 °C)

No.	Property	Value
Sample 1 (S1)	API	15
	Density (g/cm^3)	0.9658
	Dynamic viscosity (mPa·s)	650
	Asphaltene content (g/g)	0.135
Sample 2 (S2)	API	19
	Density (g/cm^3)	0.95
	Dynamic viscosity (mPa·s)	91.40
	Asphaltene content (g/g)	0.1120
Sample 3 (S3)	API	33
	Density (g/cm^3)	0.86
	Dynamic viscosity (mPa·s)	1.87
	Asphaltene content (g/g)	0.0105

tion was deoxygenated by a bubbling N_2 flow. The ammonia solution was added dropwise to adjust the pH at 11. The solution was stirred vigorously at 75 °C for 2 hours. The black precipitate was washed several times with DI-water using magnetic decantation (a permanent magnet, 0.5 T) and dried in an oven at 60 °C. To avoid developments of γ or α-Fe_2O_3 instead of Fe_3O_4 nanoparticles, no calcination treatment was used in this process [46-48].

3. Surface Modification of Fe_3O_4-NiO Nanohybrid

Surface modification of Fe_3O_4-NiO nanohybrids is required when they are used in an EOR process because Fe_3O_4-NiO nanohybrids are very unstable in water [49]. To disperse these nanohybrids in water as the cheapest and most available solvent in EOR processes, their surfaces should be hydrophilic. Deposition of nanoparticles decreases through surface modification, and less oil formation damage like permeability reduction can occur in the porous medium. Although surface modification is a key step for their use in the EM heating process, it should not affect the EM absorption ability of particles. The surface modification reduces the active surface area of nanoparticles for absorbing EM waves. Therefore, the type of modification agent is important. The optimum operational conditions of each surface modification agent, like the amount of surface modifier agent, temperature, sonication, and stirring time, were determined by the information provided in the literature and some pre-tests before each phase. A schematic of surface modification of Fe_3O_4-NiO nanohybrids with three different agents, a weak acid (like CA) [50,51], silane agent (APTES) [52,53], and polymeric compound (PEG 6000) [54,55], is shown in Fig. 1.

At first, 1 g of synthesized Fe_3O_4-NiO nanohybrids was added to DI-water. The solution was sonicated at the maximum power for 30 minutes (Fig. 1). Then, in the next stage, an appropriate amount of modification agent (2 g of CA, 4 ml of APTES, and 0.8 g of PEG 6000) was added to the solvent. The solution was stirred vigorously at a specific temperature in a given period under N_2 flow. Finally, the blackish-brown precipitates were decanted magnetically and washed three times with DI-water and dried in an oven.

4. Characterization

To identify the synthesized nanohybrids and the presence of functional groups of modification materials on their surface, Fourier transform infrared spectroscopy (FTIR, PerkinElmer Spectrum Version 10.03.06) and X-ray crystallography with Cu-Ka radiation (XRD, Philips Company JEOL JDX-803) were used. The FTIR analysis of the modified/unmodified nanohybrids was performed as solids dispersed in the KBr matrix at the ambient temperature. This analysis was carried out in the range of 4,000-400 cm^{-1} to justify the presence of modifying functional groups coated on the nanohybrid surfaces. The XRD analysis was accomplished by dried powder (at room temperature, Cu anode material, step size 0.02° and scan step time 1 second) to identify the structure of unmodified synthesized nanohybrid and to determine its crystal size. This analysis was carried out to verify the accuracy of the proposed nanohybrid synthesis method and to check for impurities in the final powder. Field emission scanning electron microscopy (FESEM, FEI NOVA FESEM 450) was performed to characterize the shape and morphology of all synthesized nanohybrids. This analysis was done by dilution of the solution, including bare and surface-modified Fe_3O_4-NiO nanohybrids, to avoid the existence of any agglomer-

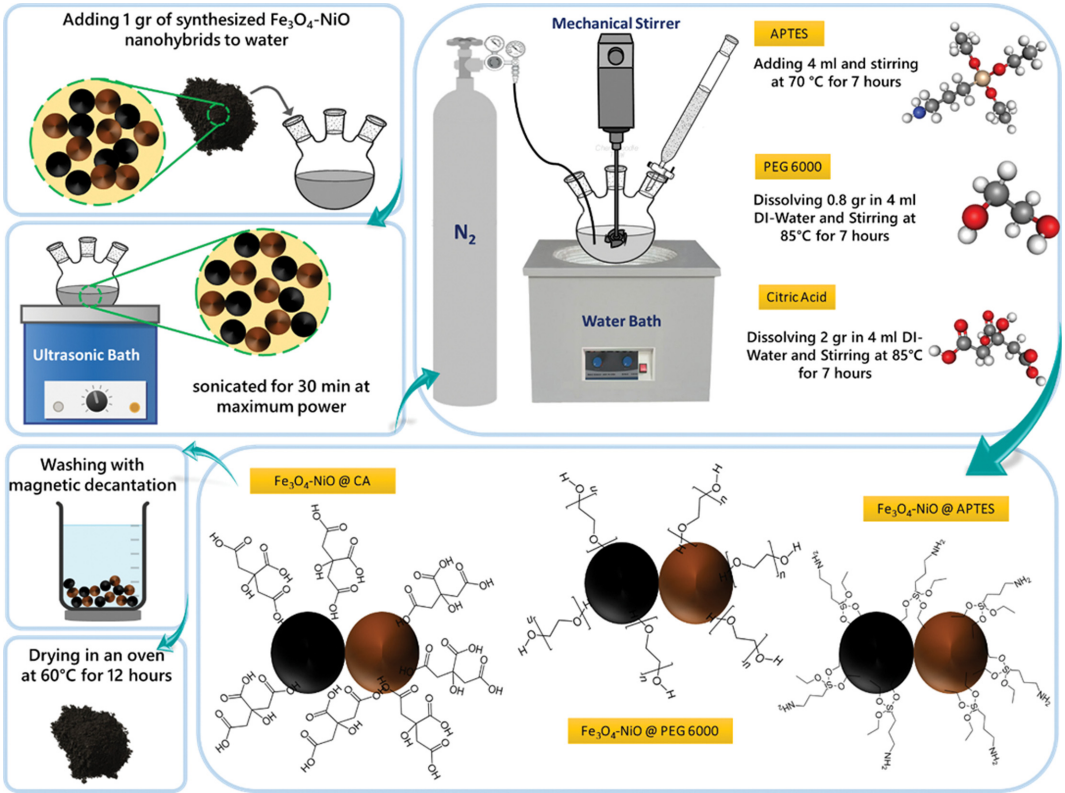


Fig. 1. The schematic of surface modification.

ated particle in the captured image. Energy dispersive X-ray spectrometry (EDX, VEGA\\-TESCAN-LMU) was used for the elemental analysis or chemical characterization of surface composition of all modified and bare powder samples. A vibrating sample magnetometer (VSM) test was applied to determine the saturation magnetization of coated/uncoated synthesized nanohybrids. This analysis was performed using solid modified/unmodified nanohybrids at room temperature over a range of applied fields from −10,000 Oe to 10,000 Oe. The stability was determined qualitatively by detecting the deposition of particles within the solution and using Zeta potential analysis over time (SZ-100 HORIBA Scientific). This analysis was also conducted at room temperature using a 0.1 wt% of each surface-modified nanohybrid dispersed in the DI-water solution.

5. The Ability of Nanoparticles to Absorb MW Energy

Two scenarios were designed to investigate the impact of surface modification on nanohybrid efficiency in the EM heating process, in order to capture heat and efficiently pass it to its surroundings. At first, 50 ml of 0.1 wt% of modified water-dispersed nanohybrids was put under 400 watt MW radiation (2.45 GHz). The temperature of the prepared samples was recorded every 30 seconds (before the evaporation point of water) using an infrared thermometer.

In the second scenario, 0.1 wt% of the hydrophobic bare nanohybrids was dispersed in 50 ml of three different crude oil samples and then placed under 400 watt MW radiation. Like the first scenario, the temperature of the prepared samples was recorded every 30 seconds using an infrared thermometer.

6. Micromodel Flooding

To study the ability of the modified nanohybrids in the EOR process under EM heating, a micromodel flooding setup was used (Fig. 2). A domestic type microwave oven (Feller MW-305) with some modification was used to generate microwaves and to allow the injection of nanofluid into the glass micromodel, operating at a frequency of 2.45 GHz and power of 900 watts (with five power levels of 10, 30, 50, 80, and 100%). To visualize the fluid flow of injected flow into the porous medium, a 2D glass micromodel with dimensions of 6×6×0.006 cm was employed. The porosity and permeability of the glass micromodel were 0.38 and 890 mD, respectively. To simulate the fluid flow into a real reservoir rock, a dolomite pore shape pattern was utilized.

For applying oil-wet conditions, similar to most carbonate oil reservoirs [56,57], the micromodel was saturated with the NaOH solution and was retrieved for 1 hour. Then, to eliminate impurities, the micromodel was washed with DI-water and dried at 200 °C for 20 minutes. In the next stage, the micromodel was fully saturated with a dilute solution consisting of 98% pure toluene and 2% trichloromethylsilane for at least 5 minutes. Finally, the micromodel was washed with methanol and then dried in the oven for 30 minutes.

After, the micromodel was fully saturated with heavy crude oil (S1). Several nanofluids with all the modified nanohybrids (0.1 wt% in DI-water) were prepared. To obtain Darcy flow conditions, the rate of nanofluid injection was adjusted at 0.07 ml/h using a high precision syringe pump. All of the injection scenarios were carried out at ambient pressure. The results of the oil recovery factor experiments were achieved by taking a snapshot from the porous medium and analyzing it using computer image processing, Photoshop software. The number of black pixels (representing the remained oil in the porous medium) before and after flooding is the basis of this method to determine the oil recovery factor. The oil recovery factor in this method was calculated by Eq. (1) [56].

$$R = \frac{S_{oi} - S_{or}}{S_{oi}} = \frac{\text{No. of black pixels in fully oil saturated} - \text{No. of black pixels after flooding}}{\text{No. of black pixels in fully oil saturated}} \quad (1)$$

where R is the recovery factor, S_{oi} as the initial oil saturation calculated by the number of black pixels of the photo in a fully oil-saturated state (before flooding operation) and S_{or} is the residual oil

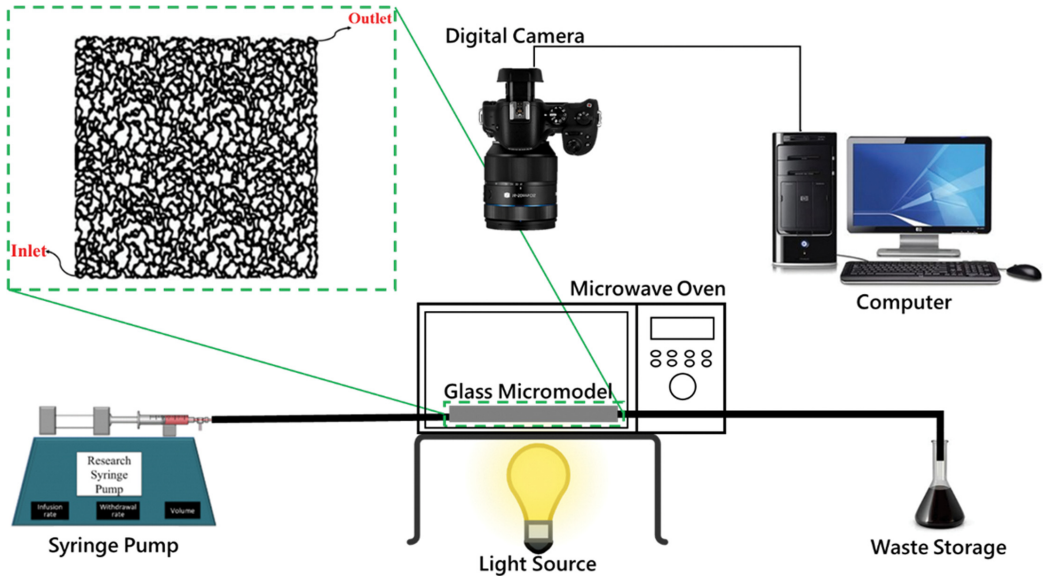


Fig. 2. Schematic of micromodel setup.

saturation (after flooding operation) obtained by counting the number of black pixels after flooding. To investigate the influence of EM heating, the porous medium was put under 400-watt MW radiation. In the MW radiation mode, only the ultimate oil recovery factor was investigated due to safety issues. To this end, after the injected fluid breakthrough, a photograph was taken and a stable state was formed in the porous medium.

7. Wettability Measurement

The wettability alteration of each nanohybrid was measured using the sessile drop technique. For this purpose, some glass panes (3×2×1 cm) were converted to the oil-wet form (regarding the detailed procedure described in section 2.6). Then, they were immersed in different water colloidal solutions prepared by individual modified nanohybrid for two days at 70 °C. Finally, the contact angle of an oil droplet on the surface was measured. The average value was reported based on the measurements made on three points of each glass.

8. Viscosity Measurement

The oil and injected fluid viscosities were measured by a rota-

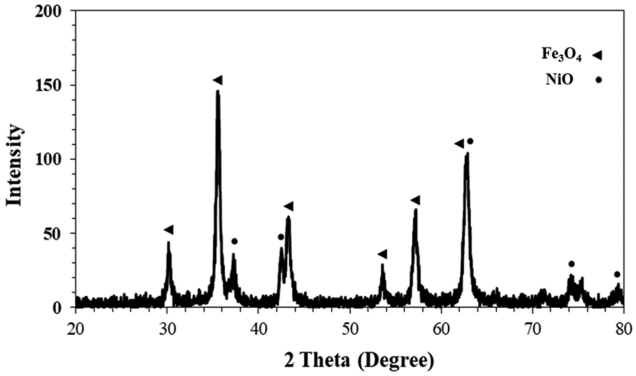
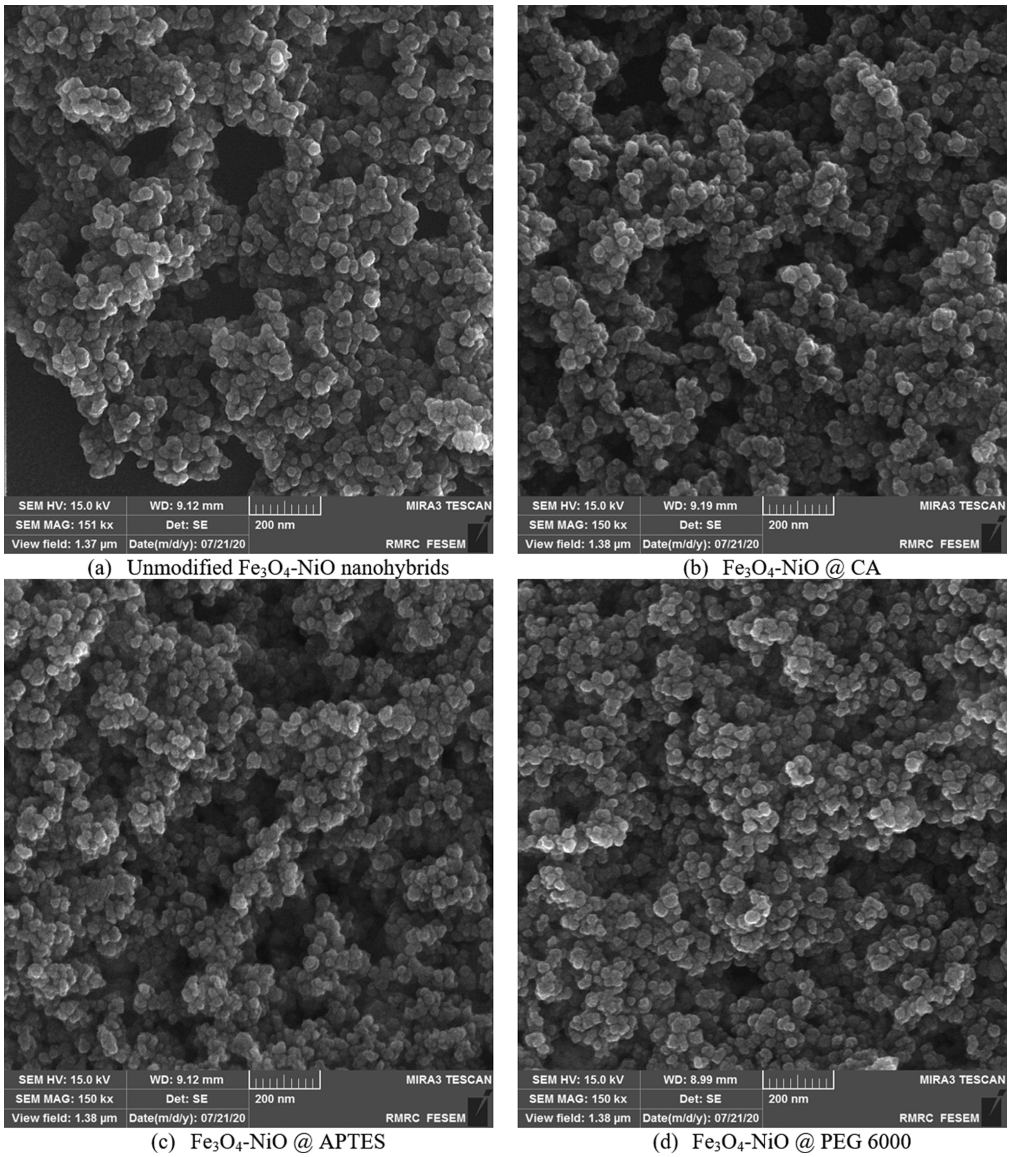


Fig. 3. The XRD pattern of uncoated Fe_3O_4-NiO nanohybrid.



(a) Unmodified Fe_3O_4-NiO nanohybrids (b) Fe_3O_4-NiO @ CA

(c) Fe_3O_4-NiO @ APTES (d) Fe_3O_4-NiO @ PEG 6000

Fig. 4. FESEM image of all bare and surface modified synthesized Fe_3O_4-NiO nanohybrid (the enlargement scale is 150000 x).

tional cylinder-cone viscometer from Anton Paar Company. All viscosity measurement tests in this study were at room temperature (25 °C). All samples were homogeneous and without air, and the amount of shear stress applied to the fluids was considered to be 500 s^{-1}. Viscosity change tests were conducted before and after the oil was exposed to the electromagnetic field. Also, the impact of adding synthesized nanohybrids to the oil samples was analyzed.

RESULTS AND DISCUSSION

1. Characterization of Synthesized Nanohybrids

Fig. 3 shows the XRD pattern of uncoated Fe_3O_4-NiO nanohybrid. The diffraction peaks at each angle correspond to an individual crystalline plane of Fe_3O_4 based on the JCPDS card No. 019-0629, and NiO based on the JCPDS card No. 047-1049. Synthesizing of nanohybrid Fe_3O_4-NiO was observed due to the absence of peaks, which was attributed to the presence of impurities. Also, the crystal size of Fe_3O_4-NiO nanohybrid determined by Scherrer's equation [44] was 21 nm.

According to the JCPDS card No. 019-0629, the diffraction peaks at 2θ=30.2°, 35.5°, 43.4°, 53.7°, 57.2°, and 62.9° correspond to (220), (311), (400), (422), (511), and (440) crystalline planes of Fe_3O_4 nanoparticles, respectively [58]. Also, the diffraction peaks at 2θ= 7.2°, 43.3°, 62.9°, 75.4°, and 79.4° correspond to (111), (200), (220), (311), and (222) crystalline planes of NiO nanoparticles (Based on JCPDS card No. 047-1049), respectively [59].

The FESEM representative image of bare and surface-modified Fe_3O_4-NiO nanohybrids is depicted in Fig. 4. This image indicates that Fe_3O_4 and NiO nanoparticles were approximately spherical. The average size of this nanohybrid was estimated at approximately 40 nm. Also, the diameter of the modified nanohybrids was increased <5-8 nm, which is not significant in a surface modification process. Therefore, the used surface modifier agents in this study had a minimum effect on the particle size of the nanohybrids. The elemental mapping of Fe, Ni, and O elements is exhibited in Figs. S1 and S2, which are presented in supporting information. These results indicate the consistent presence of these elements in the final synthesized Fe_3O_4-NiO nanohybrid over the selected region. So, in the synthesized Fe_3O_4-NiO nanohybrid with a weight ratio of 3 : 1, Fe_3O_4 and NiO nanoparticles is well distributed.

To determine the functional groups of modification agents on the surface of synthesized nanohybrid, the FTIR results of modified nanohybrids are shown in Fig. S3 (see supporting information). Regarding the results, the accuracy of the surface modification process and surface coating of the nanohybrids can be determined. The EDX results of all modified/unmodified synthesized nanohybrids to characterize elemental or chemical surface composition are illustrated in Fig. 5. Regarding this figure, the existence of Fe, O, and Ni species was confirmed in all samples, showing the synthesis of Fe_3O_4 and NiO compounds (Figs. 5(a)-(d)). The EDX analysis results of Fe_3O_4-NiO @ CA samples in Fig. 5(b) demonstrate the presence of the C element of CA on the surface of the modified nanohybrids. The observed peaks related to carbon (C), nitrogen (N), and silicon (Si) species in Fig. 5(c) confirm the presence

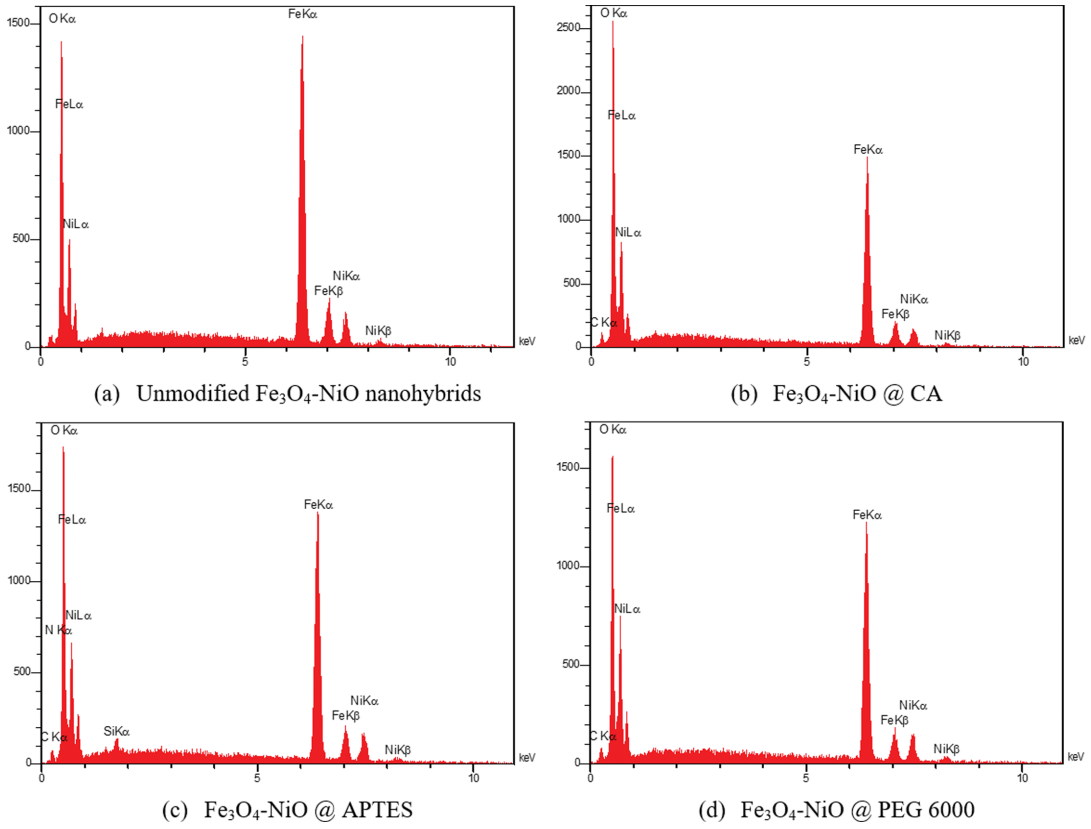


Fig. 5. EDX analysis of all modified/unmodified synthesized nanohybrids.

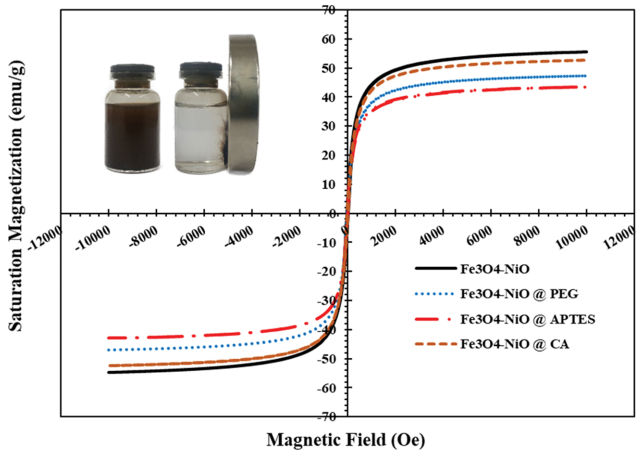


Fig. 6. VSM analysis results of coated/uncoated nanohybrids.

of APTES in the Fe_3O_4-NiO @ APTES samples. Besides, according to Fig. 5(d), the existence of C species of PEG was emphasized in the Fe_3O_4-NiO @ PEG 6000 nanohybrids.

The results of the VSM analysis of all modified and bare nanohybrids as a function of the external magnetic field from −10,000 to 10,000 Oe are presented in Fig. 6. The superparamagnetic behavior and proper magnetic responsiveness of all modified and bare nanohybrids can be obtained due to the S-shape of their VSM results.

From Fig. 6, all of the Fe_3O_4-NiO nanohybrids were separated from the solution rapidly by closing an external magnetic field to the bottle. Thus, by providing an external magnetic field on the way to the oil production line, the nanoparticles separated from crude oil quickly. The amount of saturation magnetization of uncoated Fe_3O_4-NiO nanohybrids in the mass mode is 55.44 emu/g, which is less than just Fe_3O_4 nanoparticles in that (93 emu/g). This is due to the presence of NiO particles in the synthesized nanohybrid, which has much lower magnetic properties than Fe_3O_4 nanoparticles. Besides, the surface modification reduces the magnetic performance of the nanohybrids. The effective surface area of a nanoparticle decreases after surface modification. Therefore, by exposing them to an EM field, lower EM energy can be absorbed over the surface of the nanoparticles. Thus, the surface coating acts as a shield and keeps the surface of the nanoparticles from reaching the waves. However, the type and nature of surface modification agents play a pivotal role in this reduction. Table 2 represents the coercivity and saturation magnetization threshold for all modified nanohybrids.

From Table 2, CA had the minimum effect, which decreased only 2.61 emu/g of saturation magnetization of uncoated Fe_3O_4-NiO nanohybrids. The reason for this phenomenon may be different surface modification mechanisms of CA compared to APTES and PEG, as well as the variation in the crystallinity degree and particle size [60]. Long-chain coatings, high surface density, and macromolecules of PEG and APTES on the surface of the nanohybrids through a steric stabilization mechanism increase the size and the weight of the nanohybrids [61]. In contrast, a thick and weak magnetic layer with small CA molecules has a negligible effect on the size of the nanohybrids. This highly crystalline layer has an optimal magnetization [62]. The saturation magnetization of Fe_3O_4-NiO @ PEG 6000 and Fe_3O_4-NiO @ APTES was 47.19 emu/g and 43.32 emu/g, respectively. The surface modification with all three modifying agents had a marginal impact on the coercivity and maintained their superparamagnetic behavior. In conclusion, the surface modification reduced the magnetic performance of Fe_3O_4-NiO nanohybrids, while improving the stability of nanoparticles in the injected fluid by reducing the dipolar interaction between particles. Consequently, it reduced the specific absorption rate (SAR) as a result of coating nanoparticles with a thin non-magnetic layer of modification agent [63]. Among selected modification agents in this study, CA had the least influence on the magnetic behavior of the synthesized nanohybrids [45].

Finally, the stability of nanofluids prepared with modified nanohybrids is a crucial issue for their use in an EOR process using EM heating. This factor was quantitatively investigated by Zeta potential analysis (see Table 2). Also, it was qualitatively studied by monitoring the deposition of particles within the solution (0.1 wt% in 10 ml DI-water) over time up to one week after sonication, as illustrated in Table 3.

The bare Fe_3O_4-NiO nanohybrids had a low Zeta potential. Thus, they were extremely unstable in aqueous solutions and not enough resistant to precipitate in colloidal ones. In less than 1 hour, they were deposited in the solution. By comparing Tables 2 and 3, it can be found that Fe_3O_4-NiO @ CA nanohybrids are very stable. After one week, even after a few months, no sedimentation in this colloidal solution was observed. Therefore, CA is the best modification agent with highly stable nanohybrids in aqueous solutions caused by attaching carboxylate groups of CA with two free and charged (−62.4 mV) dangling ends on the surface of bare nanohybrids [63]. It produced a negative charge by coating CA ions on the nanoparticle surfaces to improve their electrostatic stabilization and to form a Columbic repulsion force between them. Hence, the nanoparticle stability improves with minimum particle size increasing [64]. Also, it can be found that Fe_3O_4-NiO @ APTES has moderate stability (−41.8 mV Zeta potential) and Fe_3O_4-NiO @

Table 2. Magnetic properties and colloidal stability of all modified nanohybrids

Sample	Coercivity (Oe)	Saturation magnetization (emu/g)	Zeta potential (mv)	Stability behavior	Time of stability
Fe_3O_4-NiO	4.3	55.44	−13.5	Very unstable	<3 hours
Fe_3O_4-NiO @ CA	3.5	52.83	−62.4	Good stability	>one month
Fe_3O_4-NiO @ APTES	2.2	43.32	−41.8	Moderate stability	about one week
Fe_3O_4-NiO @ PEG 6000	3.7	47.19	−24.8	Low stability	<3 days

Table 3. Stability analysis of prepared nanofluids

Time (day)	Type of modified nanohybrid		
	Fe_3O_4-NiO @ CA	Fe_3O_4-NiO @ APTES	Fe_3O_4-NiO @ PEG 6000
Immediately after preparation			
1			
3			
7			

PEG 6000 nanohybrids are too unstable in a colloidal solution. Although Fe_3O_4-NiO @ APTES nanohybrids are more stable than Fe_3O_4-NiO @ PEG 6000, both of them start to deposit in the solution almost after three days. It is due to the steric stabilization of these two types of materials in comparison with CA. In steric stabilization, the nanoparticle surface is coated by a layer of macromolecules, such as polymers and long-chain molecules like amino silanes with high surface density [61]. This layer, on the one hand, serves as a barrier between the particles to be attached and increases the particle size and their tendency to precipitate.

Overall, the Fe_3O_4-NiO nanohybrids are very stable in acidic solutions like modification with CA (pH=5-6) compared to other materials such as APTES and PEG 6000 (pH=7-7.5). Therefore, it can be expected that oil formation damage problems like permeability reduction of the porous medium decrease in such circumstances.

2. MW Absorption Performance of Modified Nanohybrids

Fig. 7 shows the results of temperature variation under 400 watts MW radiation for prepared water-based nanofluids (0.1 wt%) with all modified nanohybrids. As shown in Fig. 7, by adding Fe_3O_4-NiO @ PEG to water, the rate of heating decreased compared to the water-only condition.

This phenomenon could be attributed to the non-MW absorption polymer layer formed on the surface of the nanohybrids. This layer absorbed some MW energy that was irradiated to the particles to heat itself. On the other hand, this layer increased the resistance

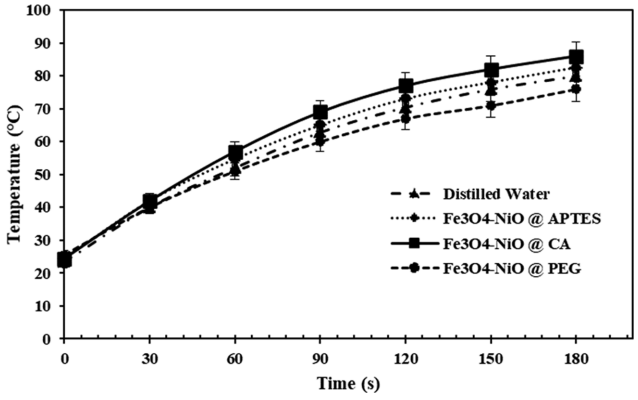


Fig. 7. Results of water-based nanofluids (0.1 wt%) temperature variation under 400 watts MW radiation.

of heating into the solution. Therefore, the rate of temperature rise was attenuated. Also, Fe_3O_4-NiO @ CA had more ability to absorb MW energy in comparison with Fe_3O_4-NiO @ APTES and heat the aqueous solutions. After 180 seconds of radiation, Fe_3O_4-NiO @ CA and Fe_3O_4-NiO @ APTES nanohybrids increased the solution temperature 6 °C and 2.5 °C more than water alone, respectively. The trend of temperature rise for these two types of nanohybrids indicated that with passing radiation time, this difference increases. Also, the small differences in the low irradiation time

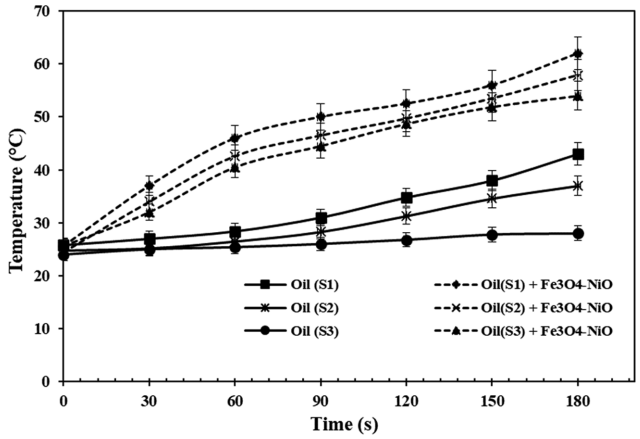


Fig. 8. Effect of adding 0.1 wt% of nanohybrids to different crude oil on the temperature rising under MW radiation.

are due to the little opportunity of the nanohybrids for absorbing and transferring MW energy to their surroundings. Therefore, it can be concluded that the type and the nature of the surface modification agent, which makes a difference in the surface modification performance of the coating material, play a pivotal role in the efficiency of absorbing MW energy by nanoparticles. The surface modification of nanoparticles improves the colloidal stability of nanoparticles to inject into oil reservoirs and reduces the useful surface area exposed to electromagnetic radiation. So, selecting the suitable surface modification agent is very important in the EM heating process. Fig. 8 illustrates the effect of adding 0.1 wt% of bare Fe_3O_4-NiO nanohybrids into different crude oil samples as a function of temperature rise under MW radiation.

Magnetic loss is the MW absorbing mechanism of all modified nanohybrids in the EM heating process. Magnetic loss heating mechanism refers to various energy dissipation inside ferromagnetic compounds like Fe_3O_4 and NiO. The time-varying magnetic field, H(t), of the microwaves makes the magnetic moments rotate inside magnetic materials. The temperature of the materials increases due to the combination of energy dissipation of generated hysteresis and eddy currents as heat inside them [65]. Moreover, dipolar polarization is another mechanism of absorbing MW energy by prepared nanohybrid solutions. Dipolar polarization is caused by the electric field component, E(t), of microwaves owing to the continuous rotation of polar molecules (DI-water) by aligning with an oscillating magnetic field. The temperature of the medium increases by pushing, pulling, and colliding the rotating molecules with other neighboring molecules. Besides, the ionic conduction mechanism in Fe_3O_4-NiO @ CA solution improves the MW absorbing efficiency compared to other modified nanohybrids. In this process, the dissipated energy as heat is due to collisions within the solution of mobile charged species (like ions).

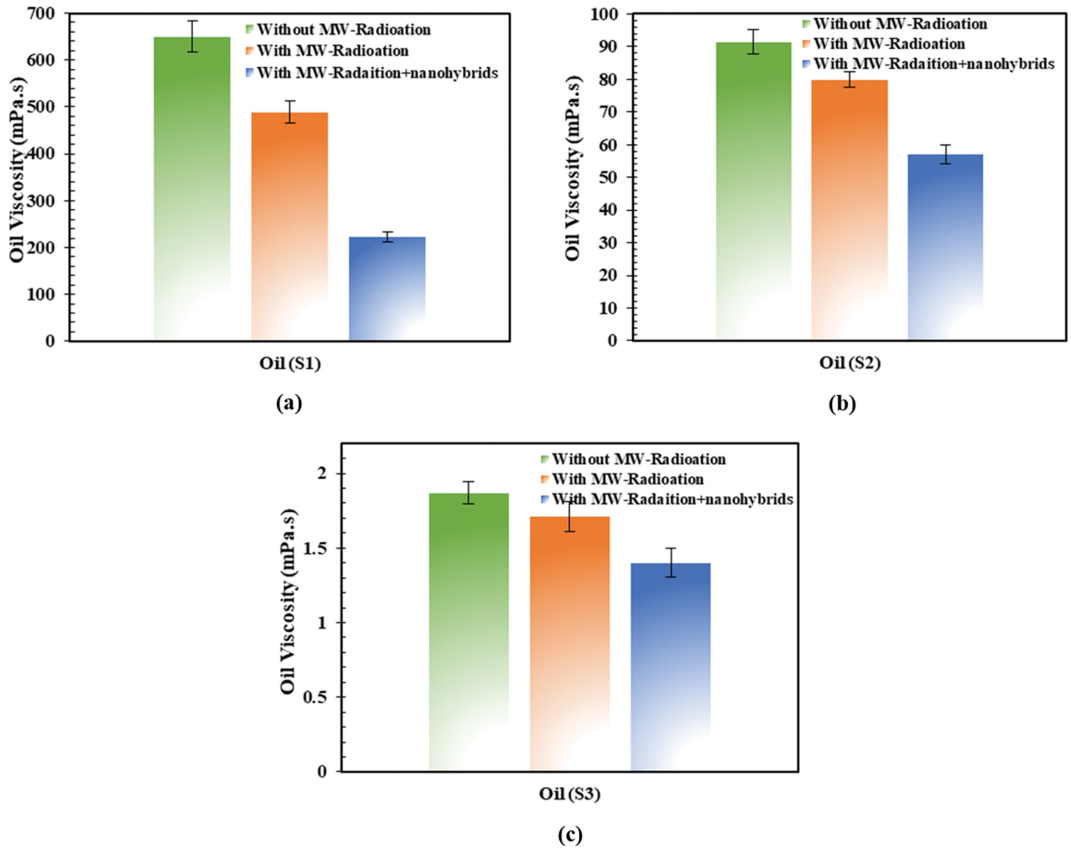


Fig. 9. Oil viscosity variation under MW radiation and adding 0.1 wt% of synthesized nanohybrids for all three oil samples, (a) oil sample (S1), (b) oil sample (S2), and (c) oil sample (S3).

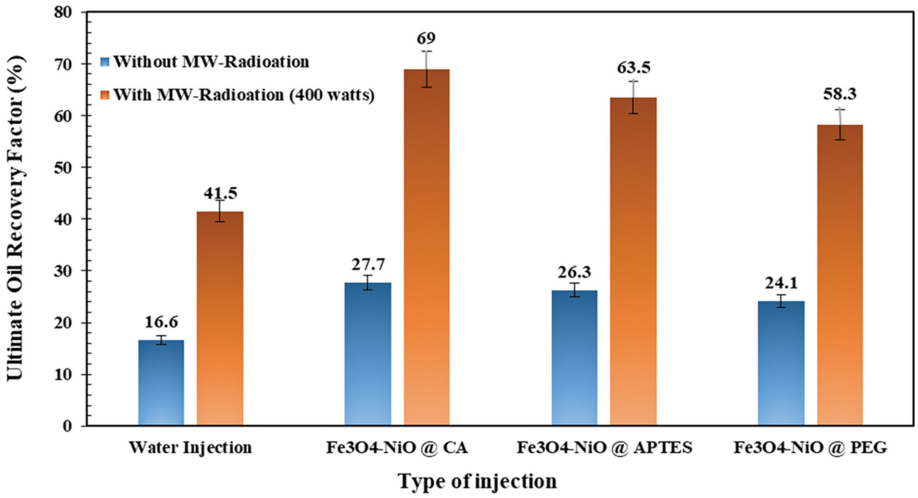


Fig. 10. Results of the ultimate oil recovery factor.

In Fig. 8, the amount of heating and the fluid temperature growth during the EM heating process relies on the type of fluid used. Oil type is an important parameter in the process of EM heating. MW radiation cannot heat the oil to the same extent. It depends on the composition of the oil and the number of its polar components, like asphaltene. For instance, heavy oil (S1) had more capacity to be heated than oil (S2) in the MW radiation process. Also, the MW radiation had a negligible effect on the heating of the light crude oil (S3). The temperature of the samples after 180 seconds of MW radiation increased on average from 25 °C to 43 °C, 37 °C and 28 °C for oil S1, S2, and S3, respectively. This shows that oil (S3) cannot absorb MW energy well. Nonetheless, by adding only 0.1 wt% of the Fe_3O_4-NiO nanohybrids, the MW absorption behavior of all oil samples was enhanced. For example, the temperature of the oil (S3) after adding 0.1 wt% of Fe_3O_4-NiO nanohybrids increased from 28 °C to 54 °C. The synthesized nanohybrids could absorb the radiated MW energy well and can transfer it to their surroundings effectively. Thus, the temperature of the oil sample increased, and due to the heating process, its viscosity decreased [66]. The results of the oil viscosity reduction by adding synthesized nanohybrids (0.1 wt%) during MW radiation are presented in Fig. 9. The viscosity of all oil samples decreased under MW radiation. In this process, the addition of the synthesized nanohybrids to oil samples helped further lessen viscosity. However, comparing Figs. 9(a)-(c) reveals that the amount of viscosity reduction of oil (S1) was greater than the others. The explanation for this effect is that this oil sample contains more polar components, such as asphaltene. Additionally, by comparing Figs. 7 and 8, it can be concluded that the aqueous solution had more ability to absorb EM wave energy than all crude oil samples due to its polar nature and OH bonds.

3. Effect of MW Radiation on Oil Recovery Factor

The results of ultimate oil recovery factors for modified nanohybrids with and without MW radiation are demonstrated in Fig. 10. As shown, MW radiation can significantly increase the heavy oil recovery factor. Water injection had only 16.6% oil recovery without any MW radiation. Nevertheless, by radiating 400 watts MW, this value increased to 41.5% (approximately 24.9% enhancement). This confirms that EM heating can help the injected fluid to improve oil extraction from heavy oil reservoirs. This increase will be further enhanced by adding modified Fe_3O_4-NiO nanohybrids to water. This involves two reasons: first, by increasing the mobility ratio of the injected fluid due to the changes in its density and viscosity, and second, the ability of nanohybrids to effectively heat crude oil by absorbing MW energy.

Mobility ratio, (M) defined as the mobility of displacing fluid (nanofluid), divided by the mobility of displaced fluid (crude oil), was calculated as follows [11]:

$$M = \frac{\lambda_i}{\lambda_o} = \frac{\left(\frac{k_i}{\mu_i}\right)}{\left(\frac{k_o}{\mu_o}\right)} = \left(\frac{\mu_o}{\mu_i}\right)\left(\frac{k_i}{k_o}\right) \quad (2)$$

where λ is the mobility of fluid phase, k is the relative permeability, μ is the viscosity. Also, i and o denote the injected fluid and oil, respectively. The viscosity of the injected fluid increased by supplementing the synthesized nanohybrids to the base fluid (water). The viscosity results of the prepared nanofluids with 0.1 wt% of

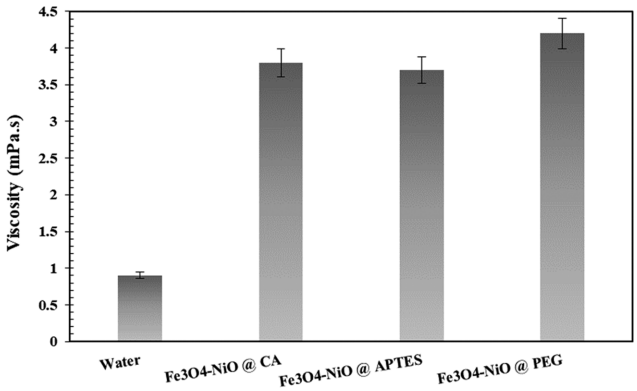


Fig. 11. Effect of nanohybrid addition on the viscosity of the injected fluid.

modified nanohybrids at 25 °C are shown in Fig. 11. From Fig. 11, the addition of synthesized nanohybrids increased the viscosity of water by about 3 mPa·s. Regarding Eq. (2), the mobility ratio decreased by increasing the viscosity of the injected fluid (μ_i) due to the addition of nanoparticles to water. The mobility ratio could be changed from an undesired value (M>1) to the desired value (M≤1), meaning that the displaced phase (oil) had higher mobility than did the displacing phase (water). Therefore, more oil could be produced from the porous medium [67]. The Fe_3O_4-NiO @ CA injection as an example of how the fluid moves at different injection times without MW irradiation is shown in Fig. S4 (see supporting information).

All the modified nanohybrids increased the oil recovery with a marginal difference and this amount increased by radiating MW energy. The Fe_3O_4-NiO @ CA, Fe_3O_4-NiO @ APTES, and Fe_3O_4-NiO @ PEG had 69%, 63.5%, and 58.3% oil recovery, respectively. These results are consistent with the findings of section 3.2. Accordingly, CA is an appropriate agent to modify Fe_3O_4-NiO nanohybrids to have high MW absorption ability and high oil recovery factor simultaneously. The microscopic images of Fe_3O_4-NiO @ CA nanofluid injection with and without MW radiation are shown in Fig. 12. The amount of trapped oil in the case of MW radiation decreased. The bubbles of vapor formed a discrete phase in the micromodel. However, by joining these bubbles together, a continuum phase formed to push the oil toward the production zone with adequate power like a piston. Besides, these bubbles increased the heat transfer surface between injected fluid and oil to enhance the efficiency of heating, and consequently, to reduce oil viscosity.

The sessile drop technique was used to measure the wettability alteration of each nanohybrid to find the reason for the difference between oil recoveries in no MW mode. The results of the oil contact angle using modified nanohybrids are shown in Table 4 and Fig. S4 in supporting information.

As shown, at first, the oil droplet was distributed on the glass completely. The contact angle was 140°. Therefore, a strong oil-wet condition could be assumed in this condition. After coating the glass with the prepared nanofluids, the oil contact angle of Fe_3O_4-NiO @ CA, Fe_3O_4-NiO @ APTES, and Fe_3O_4-NiO @ PEG was 17°, 22°, and 32°, respectively. It showed that the Fe_3O_4-NiO @ CA nanofluid had the greatest effect on the reduction of the oil contact angle. Thus, Fe_3O_4-NiO @ CA nanofluid injection could change the wettability of porous medium from strongly oil-wet to strongly water-wet. This could be related to the bonding of the carboxyl group of the CA molecules (adsorbed Fe_3O_4-NiO @CA on the glass surface) to the hydrogen bonds of the water molecules. By increasing the surface free energy, more oil can be produced from the porous medium in comparison with Fe_3O_4-NiO @ APTES and Fe_3O_4-NiO @ PEG nanofluid injection.

The fluid flows of different surface modified nanofluids as the injected fluids into the porous medium with/without MW radiation are presented in Fig. 13. Comparing Fig. 13(a)-(d), in no MW radiation mode, water had the least oil recovery factor. However, the amount of produced oil increased by adding nanohybrids to the DI-water as the base fluid, because the addition of nanohybrids changed the hydrodynamic properties of injected fluid such as density and viscosity. Therefore, the mobility ratio can be changed from an unfavorable value (M>1) to a favorable value (M≤1) and the fluid flow of injected fluid improved into the porous medium, consequently. Also, when 400 watts MW was radiated, the front part of the injected fluid became more uniform than no MW radiation mode for all the modified nanohybrids (Fig. 13(e)-(h)). For instance, for Fe_3O_4-NiO @ CA nanohybrids, there were fewer fingers of injected fluid and more surface of the micromodel was in contact with the injected fluid in the MW radiation mode (Fig. 13(f) compared to Fig. 13(b)). As a result, much oil can be produced from the porous medium. This is because the oil viscosity is reduced by absorbing MW energy through heavy crude oil (according to the results of section 3.2). The injected fluid could push the oil more easily and quickly toward the outlet port of the micromodel. Besides, the water solvent of the injected fluid was warmed up and then was evaporated (see Fig. 12). So, the mobility ratio of injected fluid improved, which means that the displaced phase

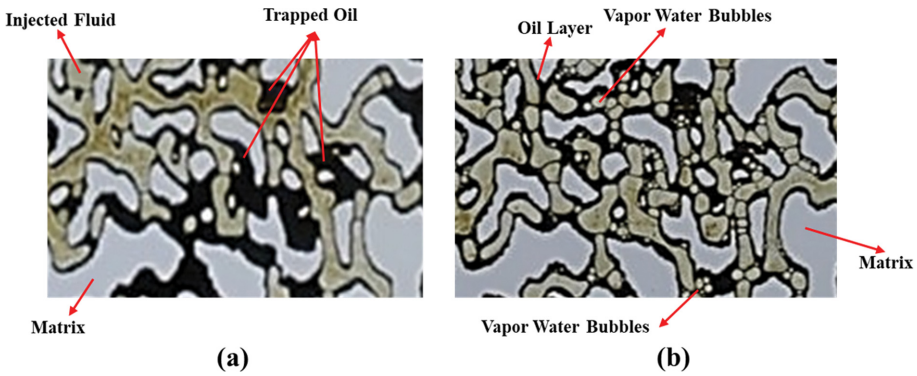


Fig. 12. Microscopic images of Fe_3O_4-NiO @ CA nanofluid injection (a) without and (b) with MW radiation (at a 10x magnification scale).

Table 4. The results of the wettability alteration

Type of fluid	Water	Fe_3O_4-NiO @ CA	Fe_3O_4-NiO @ APTES	Fe_3O_4-NiO @ PEG 6000
Oil contact angle	140°	17°	22°	32°

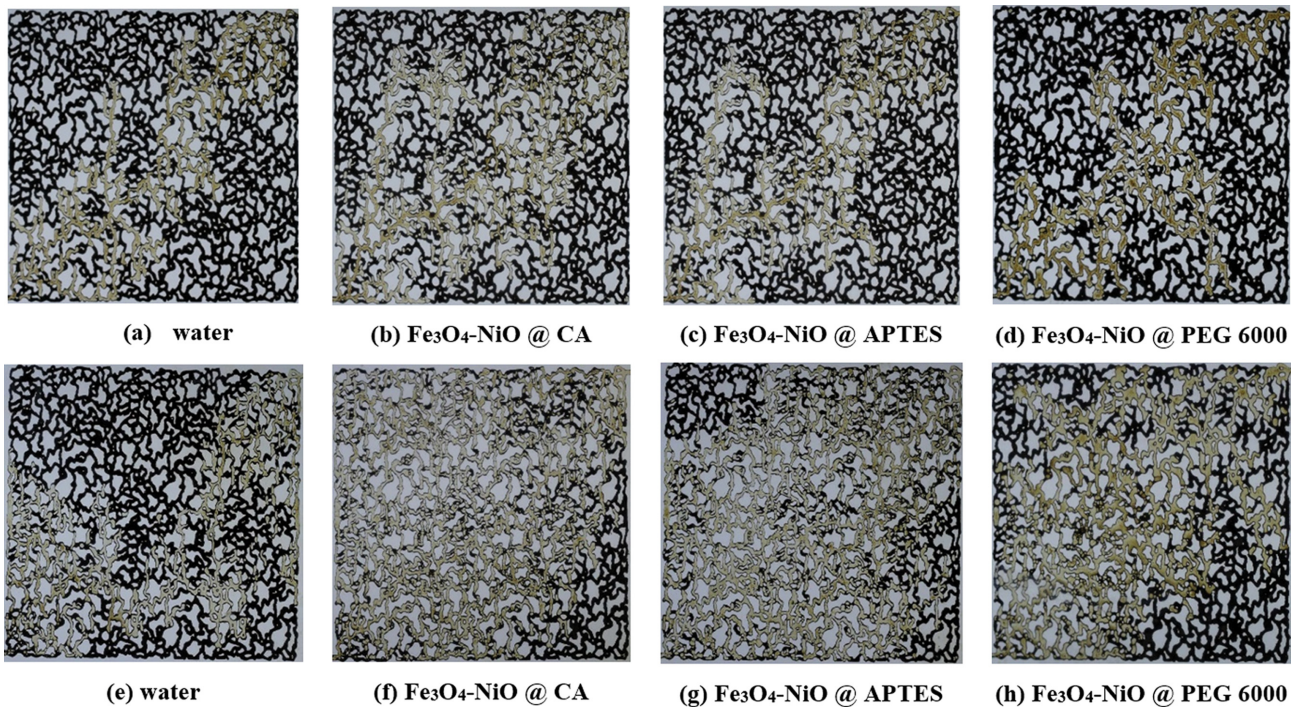


Fig. 13. The fluid flow of injected fluid into the micromodel (a)-(d) without MW radiation and (e)-(h) with 400 watts MW radiation.

(oil) had higher mobility than the displacing phase. When considering these two mechanisms (oil viscosity reduction and mobility ratio enhancement of injected fluid), the time of operation of the injection should be shortened.

CONCLUSION

The primary purpose of this study was to improve the ability of Fe_3O_4 to absorb maximum MW energy in an EM heating process for enhanced oil recovery. For this purpose, magnetic NiO nanoparticles were coupled with them through a co-precipitation method. The surface of the synthesized nanohybrids was hydrophilized using three different natural agents, including citric acid (CA), (3-aminopropyl) triethoxysilane (APTES), and polyethylene glycol (PEG 6000) to disperse in water. Synthesized surface modified nanohybrids were characterized by several analyses, such as FTIR, XRD, FESEM, EDX, and VSM. Moreover, the micromodel flooding setup was used to study the potential of synthesized nanohybrids in an EOR process. The results indicated that CA is the best agent for the simultaneous modification of superparamagnetic nanomaterials with high stability and MW absorption and oil extraction. The saturation magnetization of Fe_3O_4-NiO @ CA decreased from 55.44 emu/g to 52.83 emu/g. Microwave radiation has little effect on heating light crude oil (S3). The temperature of the samples increased from 25 °C to 43 °C, 37 °C and 28 °C for S1, S2 and S3 oil samples after 180 seconds of microwave irradiation, respectively. By adding only 0.1 wt% of unmodified Fe_3O_4-NiO nanohybrids, the microwave absorption behavior of all oil samples increased. By dispersing only 0.1 wt% of Fe_3O_4-NiO @ CA into the water, the solution temperature enhanced about 6 °C more than DI-water alone under 400 watts MW radiation after 180 seconds. The viscosity of all oil samples was decreased under MW radiation. In this process, the addition of the synthesized nanohybrids to oil samples helped further lessen viscosity. The results showed that water injection has low ability to recover residual oil in heavy and extra-heavy oil reservoirs. Although nanofluid injection increases the oil extraction coefficient, the use of nanofluid injection alone does not have a significant effect on increasing the amount of oil produced from the porous medium for such oils.

Microwave radiation significantly increased the oil recovery factor compared to the case without microwave radiation. Using 400 watts microwave radiation, oil recovery factor for water injection, injection of nanofluid containing Fe_3O_4-NiO @ CA, Fe_3O_4-NiO @ APTES, and Fe_3O_4-NiO @ PEG was increased by 24.9%, 41.3%, 37.2% and 34.2%, respectively, compared to the state without radiation. In addition, the oil contact angle of Fe_3O_4-NiO @ CA, Fe_3O_4-NiO @ APTES, and Fe_3O_4-NiO @ PEG was 17°, 22°, and 32°, respectively. It showed that the surface modified nanohybrids could change the wettability of the porous medium from oil-wet to water-wet.

ACKNOWLEDGEMENTS

The authors would like to thank Tarbiat Modares University and National Iranian Oil Company (NIOC) for financial support of this research.

SUPPORTING INFORMATION

Additional information as noted in the text. This information is available via the Internet at http://www.springer.com/chemistry/journal/11814.

REFERENCES

1. R. Gharibshahi, A. Jafari and H. Ahmadi, *J. Pet. Sci. Eng.*, **174**, 374 (2017).
2. K. Guo, H. Li and Z. Yu, *Fuel*, **185**, 886 (2016).
3. R. Hashemi, N. N. Nassar and P. P. Almao, *Appl. Energy*, **133**, 374 (2014).
4. M. Z. Hasanvand and A. Golparvar, *Pet. Sci. Technol.*, **32**, 631 (2014).
5. A. Bera and T. Babadagli, *Appl. Energy*, **151**, 206 (2015).
6. A. Neto, S. Thomas, G. Bond, F. Thibault-Starzyk, F. Ribeiro and C. Henriques, *Energy Fuels*, **28**, 2365 (2014).
7. J. Taheri-Shakib, A. Shekarifard and H. Naderi, *Fuel*, **228**, 243 (2018).
8. J. Taheri-Shakib, A. Shekarifard and H. Naderi, *J. Pet. Sci. Eng.*, **168**, 1 (2018).
9. R. Gharibshahi, A. Jafari, M. Omidkhah and J. R. Nezhad, *AIP Conf. Proc.*, **1920**, 20012 (2018).
10. S. H. Shafiai and A. Gohari, *J. Pet. Explor. Prod. Technol.*, **10**, 2923 (2020).
11. L. W. Lake, R. T. Johns, W. R. Rossen and G. A. Pope, *Fundamentals of enhanced oil recovery*, Society of Petroleum Engineers (2014).
12. A. Jafari, M. Hasani, M. Hosseini and R. Gharibshahi, *Pet. Sci.*, **17**, 434 (2020).
13. A. Mukhametshina and E. Martynova, *J. Pet. Eng.*, **2013** (2013).
14. J. Taheri-Shakib, A. Shekarifard and H. Naderi, *J. Anal. Appl. Pyrolysis*, **129**, 171 (2018).
15. J. Taheri-Shakib, A. Shekarifard and H. Naderi, *J. Pet. Sci. Eng.*, **161**, 530 (2018).
16. J. Asomaning, S. Haupt, M. Chae and D. C. Bressler, *Renew. Sustain. Energy Rev.*, **92**, 642 (2018).
17. H. Ali, H. Soleimani, N. Yahya, S. Lorimer, M. Sabet, B. M. R. Demiral and L. L. Adebayo, *J. Taibah Univ. Sci.*, **14**, 217 (2020).
18. W. Wang, C. Zhao, J. Sun, X. Wang, X. Zhao, Y. Mao, X. Li and Z. Song, *Energy*, **87**, 678 (2015).
19. M. Mozafari and Z. Nasri, *J. Pet. Sci. Eng.*, **151**, 40 (2017).
20. H. G. Yuping Duan, *Microwave absorbing materials*, Jenny Stanford Publishing, New York (2016).
21. J. Taheri-Shakib, A. Shekarifard and H. Naderi, *J. Anal. Appl. Pyrolysis*, **128**, 92 (2017).
22. J. Fianu, J. Gholinezhad and M. Hassan, *J. Pet. Sci. Eng.*, **186**, 106768 (2020).
23. J. Greff and T. Babadagli, *J. Pet. Sci. Eng.*, **112**, 258 (2013).
24. B. Hascakir, C. Acar and S. Akin, *Energy Fuels*, **23**, 6033 (2009).
25. L. Hu, H. A. Li, T. Babadagli and M. Ahmadloo, *J. Pet. Sci. Eng.*, **154**, 589 (2017).
26. H. Shang, Y. Yue, J. Zhang, J. Wang, Q. Shi, W. Zhang, L. Liu and S. Omar, *Fuel Process. Technol.*, **170**, 44 (2018).
27. R. Gharibshahi, A. Jafari, A. Haghtalab and M. S. Karambeigi, *RSC Adv.*, **5**, 28938 (2015).
28. A. Shahmohammadi and A. Jafari, *Front. Chem. Sci. Eng.*, **8**, 320 (2014).
29. H. Ali, H. Soleimani, N. Yahya, L. Khodapanah, M. Sabet, B. M. R. Demiral, T. Hussain and A. L. Lanre, *J. Mol. Liq.*, **309**, 113095 (2020).
30. M. Y. Hasibuan, S. Regina, R. Wahyu, D. Situmorang, F. Azmi, R. Syahputra, L. P. Y. Batubara, F. Prabowo, A. Setiawan and M. F. Afin, *Preprints*, 2020010115 (2020).
31. J. Taheri-Shakib, A. Shekarifard and H. Naderi, *Fuel*, **232**, 704 (2018).
32. A. Bera and T. Babadagli, *J. Pet. Sci. Eng.*, **153**, 244 (2017).
33. K. Li, B. Hou, L. Wang and Y. Cui, *Nano Lett.*, **14**, 3002 (2014).
34. Y. H. Shokrlu and T. Babadagli, *J. Pet. Sci. Eng.*, **119**, 210 (2014).
35. N. Yahya, M. Kashif, N. Nasir, M. N. Akhtar and N. M. Yusof, *J. Nano Res.*, **17**, 115 (2012).
36. N. Yahya, M. Kashif, A. Shafie, H. Soleimani, H. M. Zaid and N. R. A. Latiff, *J. Nano Res.*, **26**, 89 (2014).
37. Z. Nasri, *Chem. Eng. Process. Intensif.*, **146**, 107675 (2019).
38. Z. Nasri and M. Mozafari, *J. Pet. Sci. Eng.*, **161**, 427 (2018).
39. J. Greff and T. Babadagli, in Int. Pet. Technol. Conf., Bangkok, Thailand (2011).
40. H. Soleimani, N. Yahya, N. R. A. Latiff, H. M. Zaid, B. Demiral and J. Amighian, *J. Nano Res.*, **26**, 111 (2014).
41. H. M. Zaid, N. Yahya and N. R. A. Latiff, *J. Nano Res.*, **21**, 103 (2013).
42. K. Zhou, X. Zhou, J. Liu and Z. Huang, *J. Pet. Sci. Eng.*, **188**, 106943 (2020).
43. N. Li, G.-W. Huang, Y.-Q. Li, H.-M. Xiao, Q.-P. Feng, N. Hu and S.-Y. Fu, *ACS Appl. Mater. Interfaces*, **9**, 2973 (2017).
44. B. Sabzi dizajyekan, A. Jafari, M. Hasani, M. Vafaei-Sefti, Z. Fakhroueian and M. Baghbansalehi, *Appl. Nanosci.*, **10**, 955 (2020).
45. R. Gharibshahi, M. Omidkhah, A. Jafari and Z. Fakhroueian, *Fuel*, **282**, 118603 (2020).
46. A. Worawong, T. Jutarosaga and W. Onreabroy, *Adv. Mater. Res.*, **979**, 208 (2014).
47. A. Jafari, S. F. Shayesteh, M. Salouti and K. Boustani, *Indian J. Phys.*, **89**, 551 (2015).
48. L. Zhao, H. Yang, S. Li, L. Yu, Y. Cui, X. Zhao and S. Feng, *J. Magn. Magn. Mater.*, **301**, 287 (2006).
49. T. O. Mensah, B. Wang, G. Bothun, V. Davis and J. Winter, *Nanotechnology commercialization: Manufacturing processes and products*, John Wiley & Sons (2017).
50. L. Li, K. Y. Mak, C. W. Leung, K. Y. Chan, W. K. Chan, W. Zhong and P. W. T. Pong, *Microelectron. Eng.*, **110**, 329 (2013).
51. Y. Liu, Y. Li, X.-M. Li and T. He, *Langmuir*, **29**, 15275 (2013).
52. X.-C. Shen, X.-Z. Fang, Y.-H. Zhou and H. Liang, *Chem. Lett.*, **33**, 1468 (2004).
53. W. Wu, Q. He and C. Jiang, *Nanoscale Res. Lett.*, **3**, 397 (2008).
54. S. García-Jimeno and J. Estelrich, *Colloids Surfaces A Physicochem. Eng. Asp.*, **420**, 74 (2013).
55. A. Masoudi, H. R. M. Hosseini, M. A. Shokrgozar, R. Ahmadi and M. A. Oghabian, *Int. J. Pharm.*, **433**, 129 (2012).
56. H. A. Yousefvand and A. Jafari, *J. Pet. Sci. Eng.*, **162**, 283 (2018).
57. G. Elyaderani, M. Seyed, A. Jafari and J. Razavinezhad, *SPE J.*, **24**, 2681 (2019).
58. I. Shorstkii and N. Yakovlev, *Mater. Res. Express*, **6**, 46104 (2019).
59. A. Diallo, K. Kaviyarasu, S. Ndiaye, B. M. Mothudi, A. Ishaq, V. Rajendran and M. Maaza, *Green Chem. Lett. Rev.*, **11**, 166 (2018).
60. M. R. Ghazanfari, M. Kashefi and M. R. Jaafari, *Appl. Surf. Sci.*, **375**, 50 (2016).
61. W. Yu and H. Xie, *J. Nanomater.*, **2012**, 1 (2012).
62. S. Nigam, K. C. Barick and D. Bahadur, *J. Magn. Magn. Mater.*, **323**, 237 (2011).
63. M. E. De Sousa, M. B. Fernández van Raap, P. C. Rivas, P. Mendoza Zelis, P. Girardin, G. A. Pasquevich, J. L. Alessandrini, D.

Muraca and F. H. Sánchez, *J. Phys. Chem. C*, **117**, 5436 (2013).
64. S. Shinohara, N. Eom, E.-J. Teh, K. Tamada, D. Parsons and V. S. J. Craig, *Langmuir*, **34**, 2595 (2018).
65. J. Sun, W. Wang and Q. Yue, *Materials* (Basel), **9**, 231 (2016).
66. L. Hanyong, C. Kexin, J. Ling, W. Leilei and Y. Bo, *J. Pet. Sci. Eng.*, **170**, 374 (2018).
67. B. Peng, L. Zhang, J. Luo, P. Wang, B. Ding, M. Zeng and Z. Cheng, *RSC Adv.*, **7**, 32246 (2017).

Supporting Information

Experimental investigation of nanofluid injection assisted microwave radiation for enhanced heavy oil recovery in a micromodel system

Reza Gharibshahi*, Mohammadreza Omidkhah*,†, Arezou Jafari*,†, and Zahra Fakhroueian**

*Faculty of Chemical Engineering, Tarbiat Modares University, Tehran, Iran
**School of Chemical Engineering, College of Engineering, Institute of Petroleum Engineering, University of Tehran, Tehran, Iran
(*Received 8 July 2021 • Revised 29 August 2021 • Accepted 16 September 2021*)

1. Elemental Mapping

The results of the EDS mapping of the Fe_3O_4-NiO nanohybrid are as follows:

The elemental mapping of Fe (yellow), Ni (blue), and O (red) elements are exhibited in Fig. S2, which indicates the consistent presence of these elements in the final synthesized Fe_3O_4-NiO nanohybrid over the selected region in Fig. S1. So, as shown in Fig. S2, in the synthesized Fe_3O_4-NiO nanohybrid with a weight ratio of 3 : 1, Fe_3O_4 and NiO nanoparticles are well distributed.

2. FTIR Results

To determine the functional groups of modification agents on the surface of synthesized nanohybrid, the FTIR results of modified nanohybrids are shown in Fig. S3. The FTIR result of uncoated nanohybrids is illustrated in Fig. S3(a). In all IR spectra presented in Fig. S3, the peaks overlapped around 570-590 cm^{-1} are attributed to the Fe-O band in Fe_3O_4 and Ni-O band in NiO nanoparticles. The peaks around 3,296-3,392 cm^{-1} and 1,610-1,622 cm^{-1} can be assigned to the stretching vibration of the O-H band owing to the existence of some water in the sample. In Figs. S3(b)-(c), all labeled peaks could be ascribed to the transmittance band energy of functional groups in different modification agents. Regarding the results, the accuracy of the surface modification process and surface coating of the nanohybrids can be determined.

3. The Fluid Flow Pattern of Injected Fluid Different Injection Times without MW Irradiation

The Fe_3O_4-NiO @ CA injection as an example of how the fluid moves at different injection times without MW irradiation is shown in Fig. S4.

4. Wettability Alteration

The sessile drop technique was used to measure the wettability alteration of each nanohybrid to find the reason for the difference between oil recoveries in no MW mode. The results of the oil contact angle using modified nanohybrids are shown in Fig. S5.

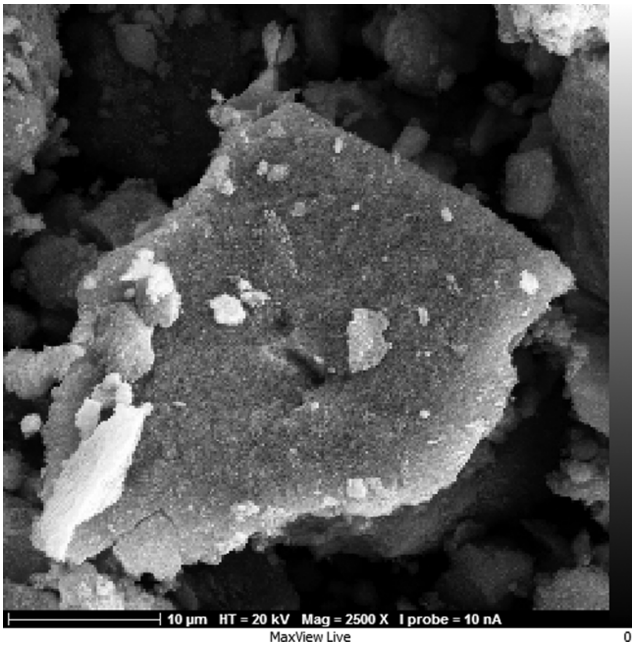


Fig. S1. FESEM image of the Fe_3O_4-NiO nanohybrid at 2500 magnification scale.

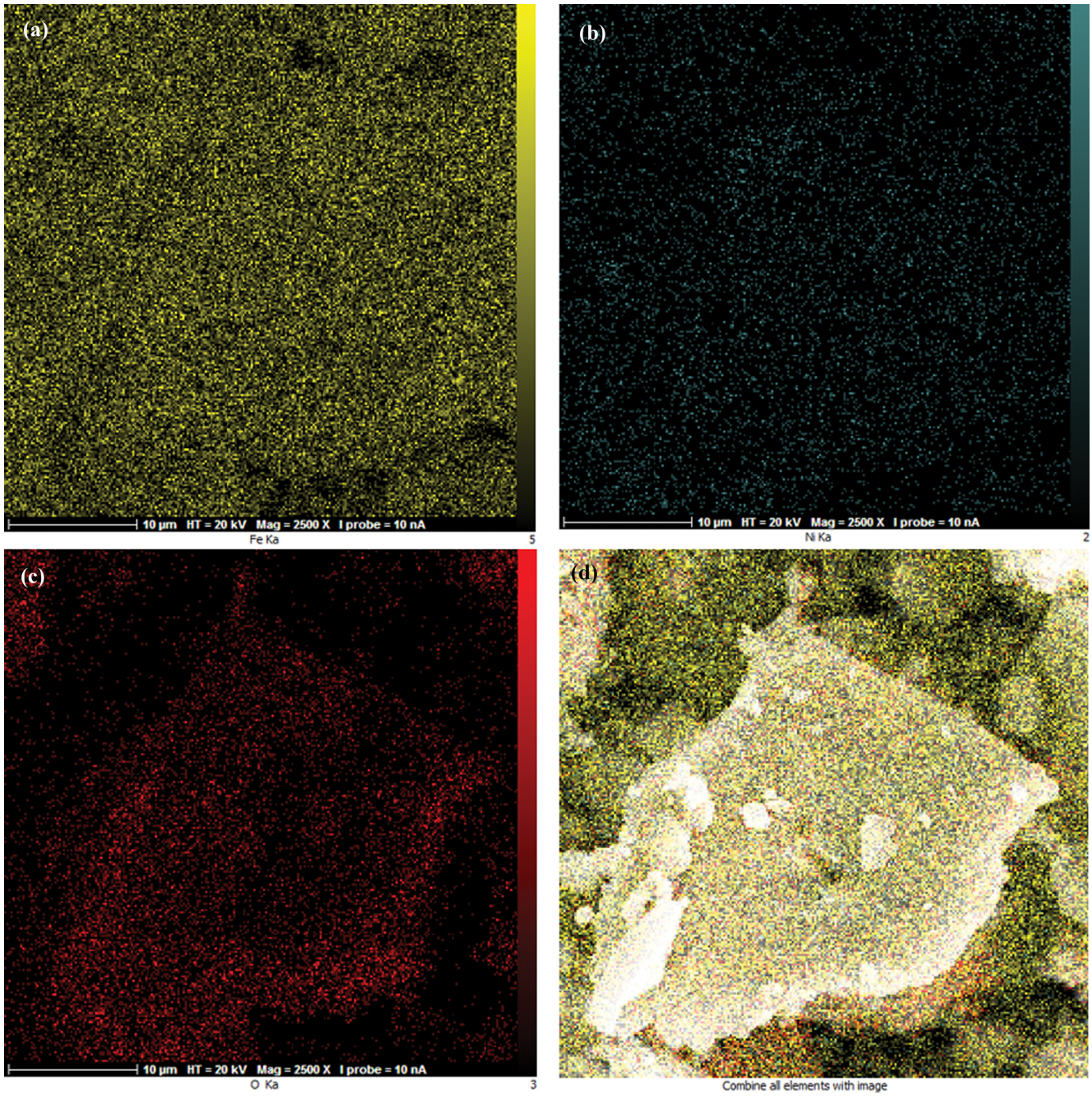


Fig. S2. Elemental mapping and Distribution patterns of (a) Fe, (b) Ni, (c) O elements, and (d) combine all elements in the synthesized Fe_3O_4-NiO nanohybrid.

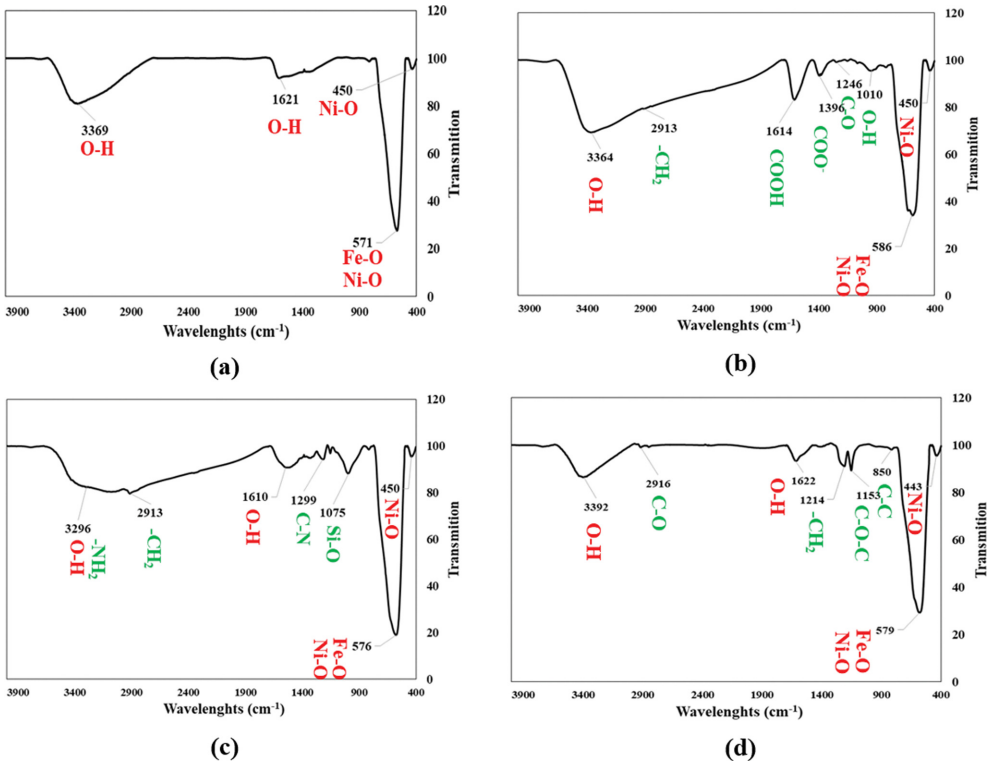


Fig. S3. The spectra of (a) bare Fe_3O_4-NiO nanohybrid and modified nanohybrid with (b) CA, (c) APTES, and (d) PEG 6000.

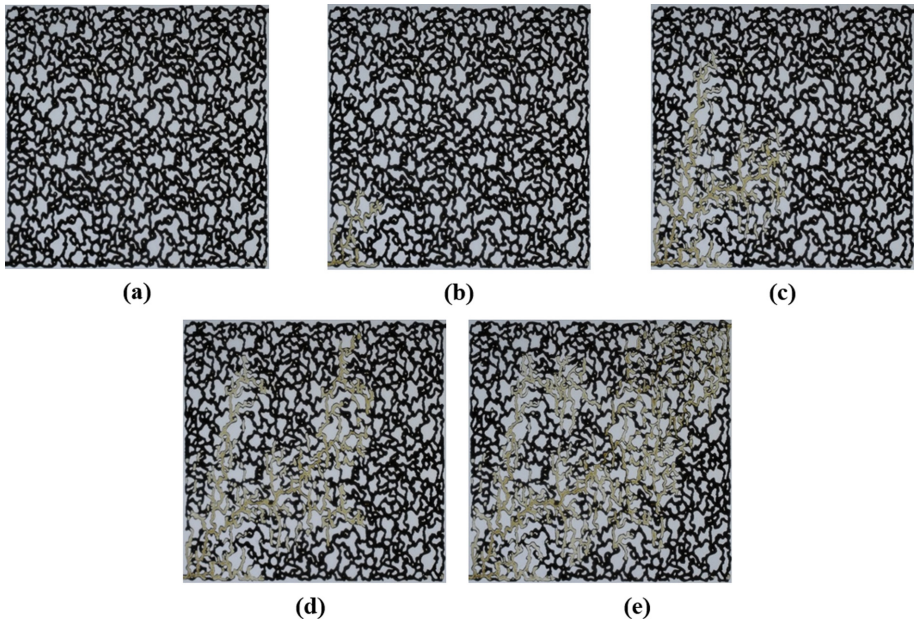


Fig. S4. The fluid flow of Fe_3O_4-NiO @ CA nanofluid at the different times of injection, (a) 0 min, (b) 20 min, (c) 40 min, (d) 50 min, and (e) 180 min.

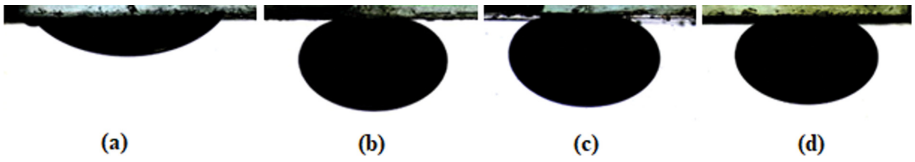


Fig. S5. The results of oil contact angle on a glass (a) water, (b) Fe_3O_4-NiO @ CA, (c) Fe_3O_4-NiO @ APTES, and (d) Fe_3O_4-NiO @ PEG 6000.